Organic Electronics 13 (2012) 1092–1099

Contents lists available at SciVerse ScienceDirect

Organic Electronics

journal homepage: www.elsevier.com/locate/orgel

Structure-properties relationships in solution-processable single-material molecular emitters for efficient green organic light-emitting diodes

Yuan Li [a], Bi-Xin Li [b], Wan-Yi Tan [a], Yan Liu [a], Xu-Hui Zhu [a,*], Fang-Yan Xie [c], Jian Chen [c], Dong-Ge Ma [b], Junbiao Peng [a], Yong Cao [a], Jean Roncali [d]

[a] State Key Laboratory of Luminescent Materials and Devices, and Institute of Polymer Optoelectronic Materials and Devices, South China University of Technology (SCUT), Guangzhou 510640, China
[b] State Key Laboratory of Polymer Physics and Chemistry, Changchun Institute of Applied Chemistry, CAS, Changchun 130022, China
[c] Instrumental Analysis & Research Center, Sun Yat-sen University, Guangzhou 510275, China
[d] Linear Conjugated Systems Group, CNRS, Moltech-Anjou, UMR 6200, University of Angers, 2 Bd Lavoisier, Angers F-49045, France

ARTICLE INFO

Article history:
Received 28 January 2012
Received in revised form 3 March 2012
Accepted 4 March 2012
Available online 23 March 2012

Keywords:
Molecular emitters
Solution processability
Organic light-emitting diodes
Green light emission

ABSTRACT

The electroluminescent properties of a series of solution-processable fluorescent molecular emitters have been systematically investigated. While the introduction of the electron-deficient benzothiadiazole unit in the structure confers efficient electron-injection on the emitter materials, they exhibit different hole-transport properties. The device characteristics of the OLEDs based on these various emitters are discussed on the basis of (i) the energy levels of their HOMO and LUMO and (ii) their hole-transport properties in relation with the charge-transport and blocking properties of the electron- and hole-transport layers.

1. Introduction

The synthesis and development of highly photoluminescent soluble organic molecular glasses remains an important research area for organic light-emitting diodes (OLEDs) [1–12]. Based on a combination of structural definition, purification feasibility and solution processability, these molecular emitting materials can contribute to the next generation of low-cost, large-area full-color displays.

The performance of an OLED depends on the intrinsic properties of the active layers as well as on the device architecture [13]. Consequently, in addition to the understanding of the electronic properties of the active emitter, a careful optimization of charge injection, transport and confinement as well as exciton blocking is critical to improving device performances.

Recently, we have reported soluble green-emitting molecular glasses leading to interesting electroluminescent (EL) properties. Thus, two-layer OLEDs devoid of hole-blocker gave green-light emission with a luminous efficiency (*LE*) of 6.0–7.0 cd A^{-1} at 20 mA cm^{-2} and CIE coordinates (0.34, 0.58) [12c].

We report here on a comparative analysis of the structure-properties relationships in a series of molecular emitters **1a**–**1c** (Chart 1). We show that the optimization of the device architecture aiming at enhancing charge recombination can greatly improve the EL performances, leading to green light emission with a luminous efficiency comparable to and/or even better than those of the vacuum-deposited devices based on green electrofluorescent small molecules [14].

* Corresponding author. Tel.: +86 20 87114346 15; fax: +86 20 87110606.
E-mail address: xuhuizhu@scut.edu.cn (X.-H. Zhu).

1566-1199/$ - see front matter © 2012 Elsevier B.V. All rights reserved.
http://dx.doi.org/10.1016/j.orgel.2012.03.001

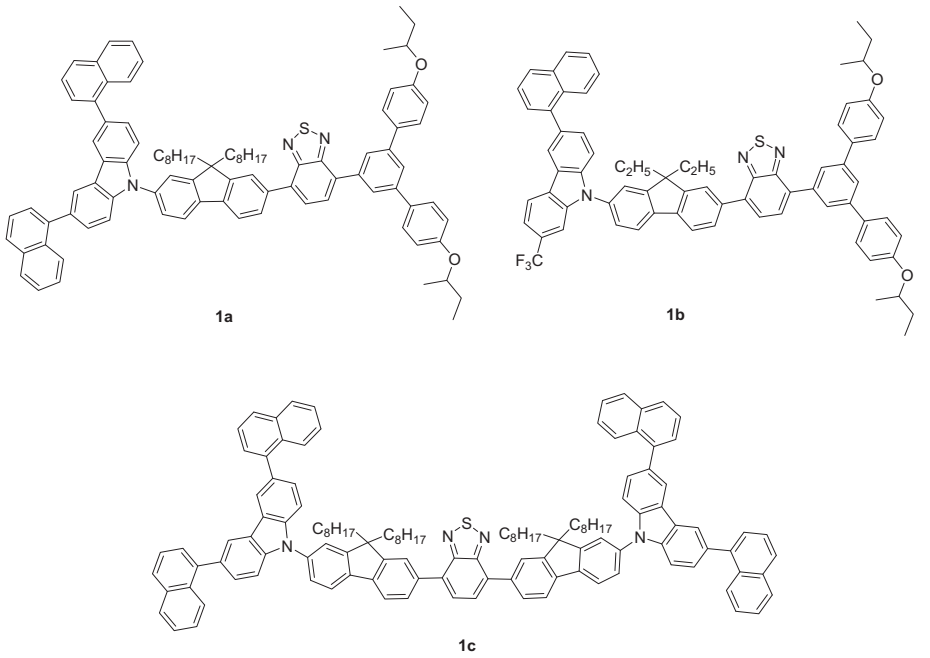

Chart 1.

2. Results and discussions

2.1. Synthesis, optical and electrochemical properties

The synthesis of compounds **1a** and **1b** has been reported earlier [12c]. Compound **1c** was obtained by a two-fold Suzuki coupling of 7-(3,6-di(1-naphthyl)carbazol-9-yl)-9,9-di-(*n*-octyl)fluoren-2-yl boronic ester with 4,7-dibromo-2,1,3-benzothiadizaole in 62% yield. The identity and purity are confirmed by ^{1}H NMR, MS and microanalysis.

The UV–vis and photoluminescence spectra of **1c** in dilute *p*-xylene solution and in solid state are shown in Fig. 1. The relevant data are summarized in Table 1, together with those for compounds **1a**/**1b**. As seen in Table 1, replacing the 3,5-di(*p*-*sec*-butoxylphenyl)phenyl end-capping group by the electron-donating moiety 7-(3,6-di(1-naphthyl)carbazol-9-yl)-9,9-di(*n*-octyl)fluoren-2-yl produces a considerable effect on the optical properties of **1c**. Thus the photoluminescent spectrum shows an emission maximum at 519 nm in solution (ϕem = 0.73), shifting to 536 nm for solution-cast thin solid films (ϕem = 0.56), leading to yellow-green light emission.

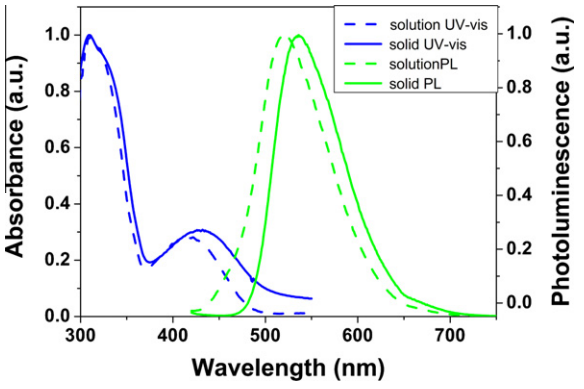

Fig. 1. UV–vis and PL spectra of **1c** in *p*-xylene solution and as films cast on quartz (PL, excited at 422 nm).

The cyclic voltammogram of compound **1c** shows a reversible reduction wave at ca. −1.89 V, and a quasi-reversible oxidation with an anodic peak potential of 0.81 V vs. Fc^+/Fc, similar to that of compound 1a (Table 1 and Fig. 2). The HOMO levels derived from UPS measurements are ca. −5.9 eV for thin films of **1a** and **1c** and −6.2 eV for **1b**, the latter having a strong electron-withdrawing trifluoromethyl substituent on the carbazolyl ring (See SI: Fig. S1). Note that the reported HOMO level of 4,4′-bis(carbazol-9-yl)biphenyl) was 6.0 eV [15]. Based on the HOMO levels and the onset of the solid-state electronic absorptions, the LUMO levels of compounds **1a**–**1c** are estimated to be −3.3 to −3.6 eV.

2.2. Electroluminescent properties

Two main types of OLEDs consisting of compounds **1a**–**1c** as solution-processed emitters have been fabricated. The electron-transport layer Alq_3, TPBI (ETL), LiF and Al are vacuum-deposited. For compound **1b**, double electron-transport layers (ETLs) BCP(10 nm)/Alq_3(20 nm) have been used to achieve hole confinement.

Type I: ITO/PEDOT: PSS(50 nm)/**1a**–**1c**(45 nm)/ETL (30 nm)/LiF(1.5 nm)/Al(200 nm)

Type II: ITO/PEDOT:PSS(50 nm)/PVK(40 nm)/**1a**–**1c**(45 nm)/ETL(30 nm)/LiF(1.5 nm)/Al(200 nm).

The respective HOMO and LUMO levels of the emitters and charge transport/blocking materials are shown in Scheme 1.

Table 1
UV–vis, photoluminescence emission and cyclic voltammetric data for compounds **1a**–**1c** [12c].

	UV–vis[a] (λ_{max}^{abs}, nm)		PL[a] (λ_{max}^{em}, nm; f_{em})		E_{pa}[d] (V)	E_0[d] (V)	HOMO[e] (eV)	LUMO[f] (eV)
	Solution	Solid	Solution[b]	Solid[c]	Reduction	Oxidation		
1c	307, 422	309, 432	519 (0.73)	536 (0.56)	−1.89	0.81	−5.9	−3.4
1a	302, 408	285, 413	504 (0.67)	518 (0.72)	−1.87	0.81	−5.9	−3.3
1b	300, 400	301, 413	500 (0.58)	521 (0.51)	−1.86	1.04	−6.2	−3.6

[a] In *p*-xylene.
[b] $\sim 10^{-6}$ Mol L^{-1} in *p*-xylene using quinine bisulfate in 0.1 *N* H_2SO_4 as the reference ($\phi_r = 0.54$).
[c] Measured in an integrating sphere under 325 nm laser excitation.
[d] Derived from cyclic voltammetry vs. Fc^+/Fc.
[e] Measured by ultraviolet photoelectron spectroscopy (UPS).
[f] Derived from the HOMO level and onset of thin film electronic absorption.

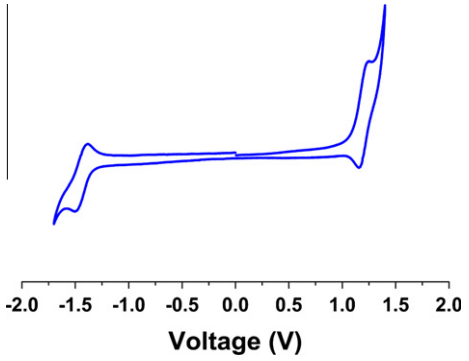

Fig. 2. Cyclic voltammogram of compound **1c** in 0.10 M *n*-Bu_4NPF_6 in 5:1 CH_2Cl_2/CH_3CN. Reference electrode: Ag/AgCl, scan rate: 50 mV s^{-1}.

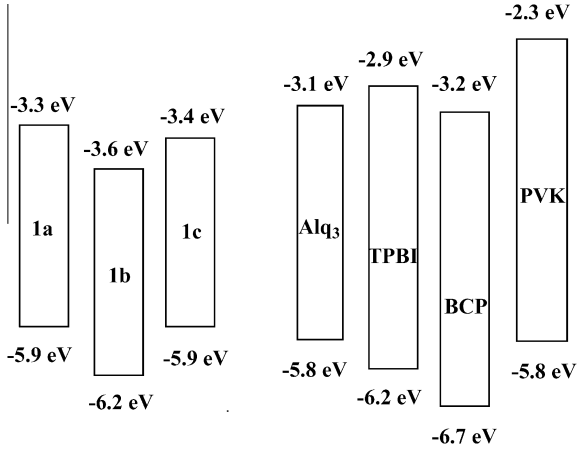

Scheme 1. Schematic illustration of HOMO and LUMO levels of compounds **1a**–**1c** and charge transport/blocking materials. Alq_3 = tris(8-hydroxyquinoline)aluminum, TPBI = 1,3,5-tris(*N*-phenyl-benzimidizol-2-yl)-benzene, BCP = 2,9-dimethyl-4,7-diphenyl-1,10-phenanthroline and PVK = poly(*N*-vinylcarbazole).

2.2.1. Electron-only devices based on the electron-transport layers (ETLs)

The electron-only devices based on ETLs have been fabricated in order to have a first understanding of their effect on the EL performances: ITO/BCP(10 nm)/ETL/LiF (1.5 nm)/Al, where ETL = TPBI(30 nm), Alq_3(30 nm) and BCP(10 nm)/Alq_3(20 nm), respectively. The current density (*J*)-voltage (*V*) characteristics are shown in Fig. 3.

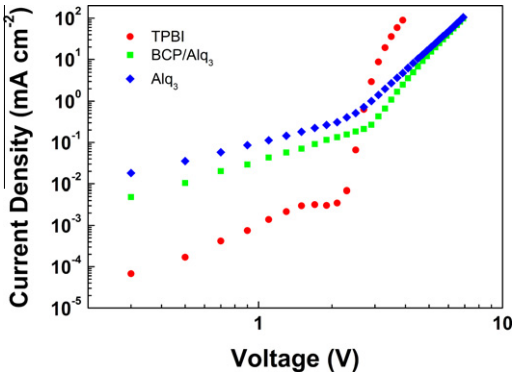

Fig. 3. *J*–*V* characteristics of electron-only devices: ITO/BCP(10 nm)/ETLs/LiF(1.5 nm)/Al, where ETLs = TPBI (30 nm), Alq_3 (30 nm) and BCP (10 nm)/Alq_3(20 nm), respectively. The active area is 9 mm^2.

The Alq_3-based single-carrier device consistently shows a higher electron current density over the BCP/Alq_3-based device over the entire voltage range. At high voltage, the electron current density of both the devices becomes very close.

For an applied bias above 2.1 V, the electron current density of the TPBI-based device increases very rapidly and reaches the highest over ~2.8 V. The differences in the *J*–*V* characteristics of the electron-only devices reflect the variability of the electron injection properties of these ETLs and agree well with their electron mobilities reported previously [16].

2.2.2. OLEDs based on compound 1c (Type I)

The device characteristics of **1c** with Alq_3 and TPBI as the ETL are shown in Fig. 4. The turn-on voltage defined at a luminance of ~1 cd m^{-2} was ~3.7 and 4.1 V for the Alq_3 and TPBI devices, respectively.

As shown in Fig. 4a, the Alq_3 device exhibits a larger current density over the entire voltage range, whilst the TPBI device should have better electron injection at high voltage (Fig. 3). This observation indicates that soon after the OLED is turned on, hole current appears to be dominant in the emitting layer with hole leakage into the Alq_3 layer (Scheme 1), leading to the lowering of the device efficiency

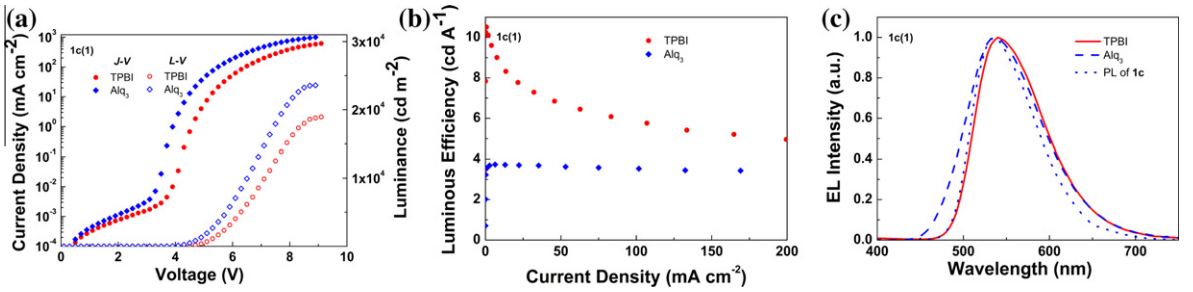

Fig. 4. (a) *J–V–L* characteristics of the OLEDs: ITO/PEDOT:PSS/1c/ETL/LiF/Al, where ETL = TPBI and Alq_3, respectively. (b) *LE–J* characteristics. (c) EL spectra, together with the PL emission of **1c** in thin solid film.

and broadening of the EL emission due to the contribution of the Alq_3 emission (Fig. 4b and c).

It is important to note that the main EL emission in the Alq_3 device arises from **1c**, resembling the PL emission (Fig. 4c), which suggests that charge recombination nevertheless occurs largely in the active emitting layer (EML) with electron injection facilitated by its low LUMO level (**1c**: $E_{LUMO} = -3.4$ eV).

The introduction of a TPBI layer, which simultaneously provides hole confinement by increasing the hole-transport barrier across the EML/ETL interface and improves electron injection with increasing voltage, leads to a large enhancement of EL efficiency. Thus a maximal luminous efficiency of 10.5 cd A^{-1} (at 0.68 mA cm^{-2} and 4.5 V) is achieved. At -20 mA cm^{-2} (5.5 V), $LE = 7.8$ cd A^{-1} vs. 3.7 cd A^{-1} for the Alq_3 device.

2.2.3. OLEDs based on compound 1b (Type I)

The device characteristics of **1b** are shown in Fig. 5. With respect to **1c**, the presence of a CF_3 moiety on the carbazolyl ring results in a considerably higher turn-on voltage of ~4.7 and 4.9 V for the Alq_3 and TPBI OLEDs, respectively.

As seen from Fig. 5c, besides an emission maximum at ca. 520 nm, the occurrence of a weak emission around 390 nm, which is absent in the Alq_3 OLED, is assigned to the TPBI emission. Thus, in contrast to **1c**, the deep HOMO level of **1b** contributes to incomplete hole confinement in the TPBI OLED. Nevertheless, it still shows a maximal luminous efficiency of ~6.3 cd A^{-1} at ~9.2 mA cm^{-2} (6.1 V). At ~20 mA cm^{-2}, $LE = 6.27$ cd A^{-1} (−6.5 V), close to that of the OLED device with Ba/Al as the cathode [12c].

The leakage of hole current into the Alq_3 layer is anticipated in the Alq_3 OLED. Unlike **1c**, on the sole basis of the EL spectrum it is difficult to distinguish whether the majority of the EL emission arises from the emitting layer or from the Alq_3 layer. However, the Alq_3 OLED shows stable green light emission with CIE coordinates (0.32, 0.57) and a maximal luminous efficiency of ca. 6.1 cd A^{-1} at ca. 56 mA cm^{-2}.

Consequently, incorporating a thin layer of BCP between the EML and Alq_3 layer gives rise to hole confinement due to an increasing hole-injection barrier of −0.5 V at the EML/ETL interface (BCP: $E_{HOMO} = -6.7$ eV). No emission of BCP around 490 nm is observed [17]. It occurs surprisingly that the BCP/Alq_3 OLEDs repeatedly show inferior luminous efficiency (Fig. 5b). For instance, at ~20 mA cm^{-2}, $LE = 5.4$ cd A^{-1}, vs. −6.0 and 6.27 cd A^{-1} for the Alq_3 and TPBI OLEDs, respectively. This observation reveals that hole current in the neat film of compound **1b** is only modestly dominant. While hole confinement contributes to improving device efficiency, it seems that electron injection might be still the limiting factor in this case.

2.2.4. OLEDs based on compound 1a (Type I)

The device characteristics of **1a** are shown in Fig. 6. The Alq_3 and TPBI devices show respectively a turn-on voltage of 4.5 and 4.7 V, which is intermediate between that of the corresponding **1b**- and **1c**-based OLEDs.

As in the case of **1c**, the higher current density in the Alq_3 device over the TPBI device (Fig. 6a) supports that hole current prevails in the emitting layer over the turn-on voltage. Noticeably, the EL performance of the Alq_3 device appears more favorable than that of the **1c**-based Alq_3 OLED:

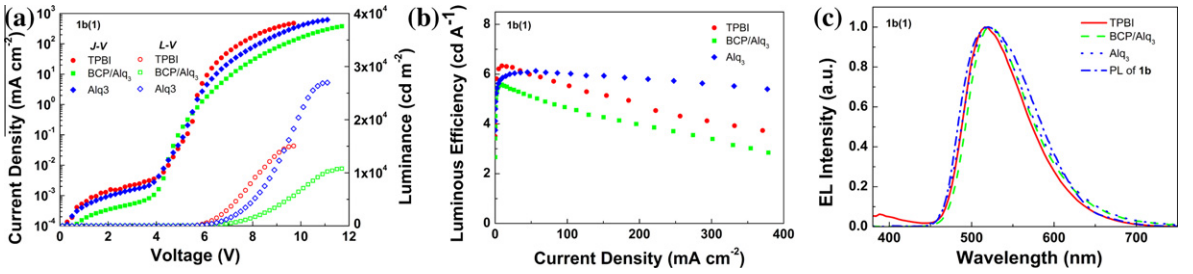

Fig. 5. (a) *J–V–L* characteristics of the OLEDs: ITO/PEDOT:PSS/**1b**/ETLs/LiF/Al, where ETL = TPBI, BCP/Alq_3 and Alq_3, respectively. (b) *LE–J* characteristics. (c) EL spectra, together with the PL of **1b** in thin solid film.

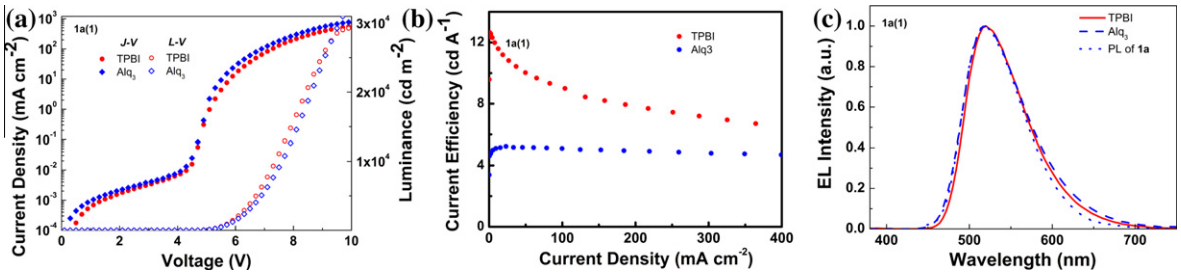

Fig. 6. (a) *J–V–L* characteristics of the OLEDs: ITO/PEDOT:PSS/**1a**/ETL/LiF/Al, where ETL = TPBI and Alq_3, respectively. (b) *LE–J* characteristics. (c) EL spectra, together with the PL of **1a** in thin solid film.

λ_{max} = 520 nm, CIE coordinates (0.31, 0.57), LE_{max} = 5.2 cd A^{-1} at ~23 mA cm^{-2} (5.9 V), while comparable to that of the **1b**-based Alq_3 OLED.

Pure green EL emission arising from **1a** is thus successfully realized in the TPBI device. The OLED performance is greatly improved: LE_{max} = 12.6 cd A^{-1} (at ~1.0 mA cm^{-2}), λ^{EL}_{max} = 520 nm with CIE coordinates (0.31, 0.59), which are very close to the EBU color gamut green point CIE (x = 0.29, y = 0.60). At ca. 20 mA cm^{-2} (6.1 V) and 100 mA cm^{-2} (7.3 V), *LE* remains at ~11.2 cd A^{-1} (L = 2090 cd m^{-2}) and 9.0 cd A^{-1} (L = ~9300 cd m^{-2}), respectively.

For comparison the **1c**-based TPBI device produces yellow-green light emission with CIE coordinates (0.39, 0.57). The device efficiency drops more rapidly with increasing current density: $LE \approx 7.8$ cd A^{-1} at ~20 mA cm^{-2} and decreases to 5.7 cd A^{-1} at 100 mA cm^{-2}.

The analysis of the device characteristics of the above OLEDs suggests an excess of hole current in the emitting layer over the turn-on voltage (Figs. 4–6). Due to a potentially large hole injection barrier at the PEDOT:PSS/EML interface, hole injection might possibly be limited in these OLEDs at low voltages and need further investigation [18]. On the other hand, there is no electron-injection barrier at the ETL/EML interfaces. Thus, the differences in the *J–V* characteristics of the respective TPBI and Alq_3 OLED series at the stage when the devices are turned on, i.e. $J_{1c} > J_{1a} > J_{1b}$ (**see** SI: Fig. S2) may reflect in a large part the hole transport properties of the active emitters, which is supported by the hole-only devices (Fig. 7) [19].

2.2.5. OLEDs based on compounds ***1a–1c*** (Type II)

In order to further increase the device efficiency, a PVK layer is introduced between the PEDOT:PSS and EML, which possesses a generally low hole mobility (~10^{-7} cm^2 V^{-1} s^{-1}) [20,21], thus decreasing hole injection into the EML.

A highest efficiency increase is noted for the yellow-green emitter **1c**. For instance, a maximum luminous efficiency of 14.3 cd A^{-1} with CIE coordinates (0.38, 0.59) is achieved in the OLED consisting of TPBI as the ETL. At ~20 and 100 mA cm^{-2}, $LE \approx 11.1$ and 8.7 cd A^{-1}, respectively (Fig. 8c). As an indication of the reduced hole current in the EML, an increase of the device efficiency accompanied by a narrowing of the EL emission is witnessed in the resulting Alq_3 OLED, which suggests less hole leaking into the Alq_3 layer and thereby an enhancement of exciton formation in the active emitting layer (Fig. 8e).

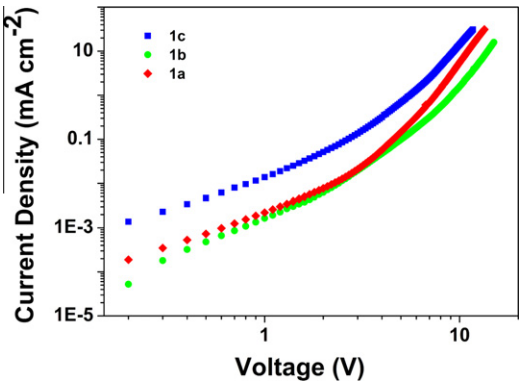

Fig. 7. *J–V* characteristics of the hole-only devices: ITO/PEDOT:PSS (50 nm)/**1a–1c** (80 nm)/MoO_3 (6 nm)/Al (200 nm). MoO_3 serves as an electron-blocking layer. The active area of the devices is 16 mm^2. The current density for compounds **1a–1c** follows a power law ($J \propto V^m$) with ~1.2 < m < ~3 at low voltages (below ~3 V for **1a**/**1b** and ~4 V for **1c**) and $m \approx 5.5 \pm 0.5$ at high voltages. This observation is characteristic of the bulk-limited carrier transport for low-mobility molecular glasses with traps in the films.

In the case of **1b**, besides a dominant emission peak at 524 nm, the TPBI OLED still shows a weaker emission band around 380 nm as observed earlier (see SI: Fig. S3). Nevertheless, a maximal luminous efficiency of ~7.5 cd A^{-1} is obtained (at ~3.8 mA cm^{-2}) with CIE coordinates (0.31, 0.59). At ~20 mA cm^{-2}, *LE* remains at 7.0 cd A^{-1}. On the other hand, it is worth noting that the luminous efficiency of the Alq_3 OLED with a PVK layer is further increased to ~7.0 cd A^{-1} at ~9.6 mA cm^{-2}. At ~20 and 100 mA cm^{-2}, *LE* remains at 6.9 and 6.1 cd A^{-1}, respectively. The redshift of the EL emission leading to λ^{EL}_{max} at 532 nm and CIE coordinates (0.34, 0.58) is also observed for **1a**-based Alq_3 OLED.

Finally, a luminous efficiency of ~13.4 cd A^{-1} for compound **1a** has been observed in the resulting TPBI OLED. At ~20 mA cm^{-2}, *LE* remains at 11.7 cd A^{-1} and decreases to 9.5 cd A^{-1} at 100 mA cm^{-2} (L = 10247 cd m^{-2}, Fig. 8d). The slower efficiency roll-off with increasing current density is attributed to the smaller hole current in the emitting layer, with respect to compound **1c** (Fig. 7). In addition, the EL emission is stable in a wide voltage range with λ^{EL}_{max} at 520 nm and CIE coordinates (0.31, 0.60) (Fig. 8f). Consequently, the high device efficiency combined with pure green EL emission and synthetic accessibility brings compound **1a** among the best solution-processable single-material green fluorescent molecular emitters [5b,7,10].

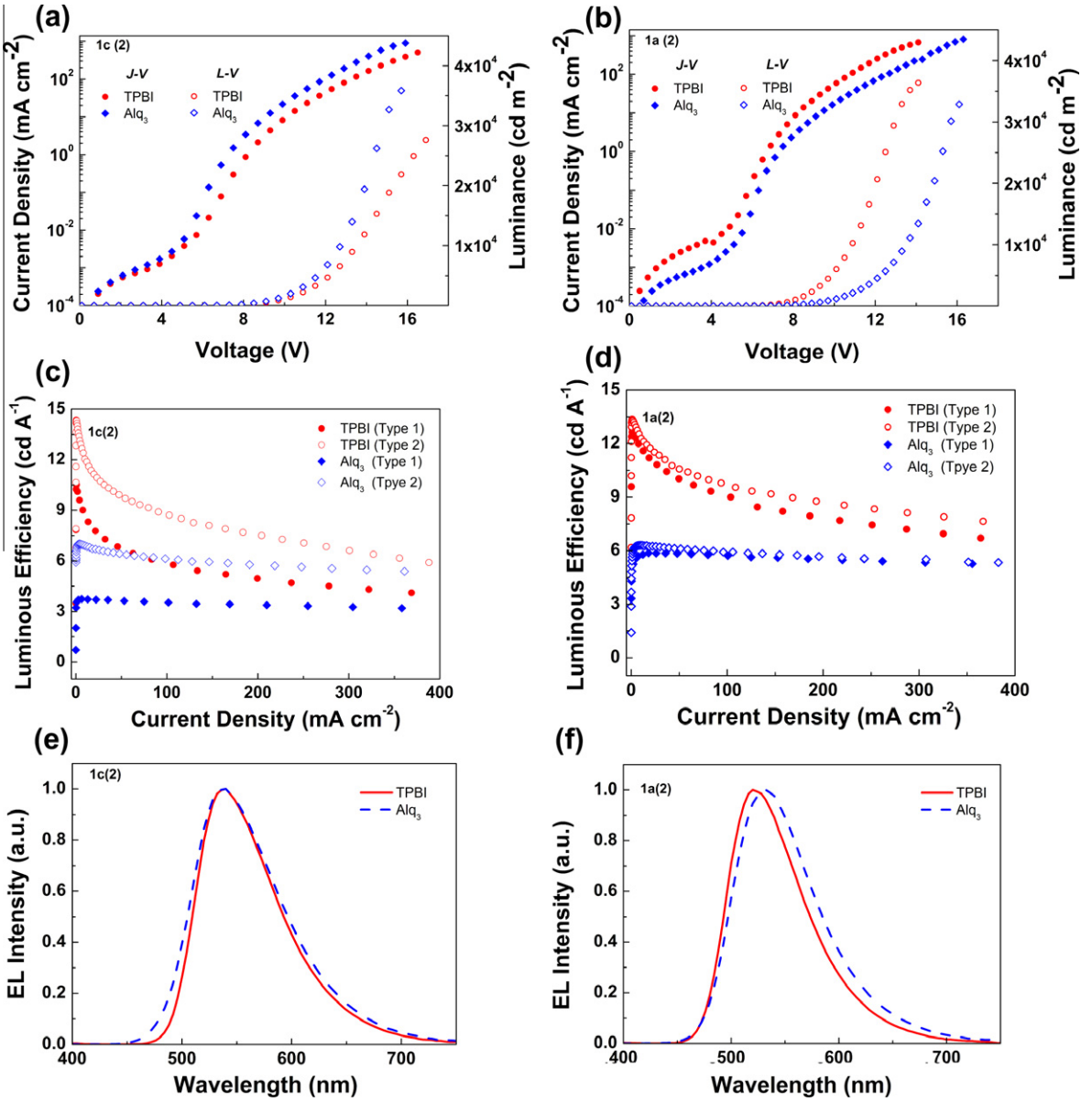

Fig. 8. Device characteristics of the OLEDs (Type II): ITO/PEDOT:PSS/PVK/EML/ETL/LiF/Al, where EML = **1a** and **1c**, ETL = TPBI and Alq_3, respectively. (a and b) *J–V–L* characteristics. (c and d) *LE–J* characteristics. (e and f) EL spectra. *LE–J* characteristics of the OLEDs without a PVK layer are provided.

3. Conclusions

In summary, efficient electroluminescence has been realized based on solution-processed single-material green and yellow-green molecular emitters. In addition to enabling hole confinement and restricting hole injection, the low LUMO levels of the active emitters in combination with the high electron-injection property of the electron-transport layer improves charge recombination and thereby device efficiency, since hole current is generally dominant over the turn-on voltage in the present OLEDs. Notably, a high luminous efficiency of 11.7 cd A^{-1} at 20 mA cm^{-2} with CIE coordinates (0.31, 0.60) and a low efficiency roll-off is obtained for the unsymmetrical green emitter comprising 3,6-bis(1-naphthyl)carbazolyl and 3,5-bis(*p*-alkyloxylphenyl)phenyl end groups. Furthermore, the results presented here offer valuable structure-properties relationships concerning this series of molecular emitters and should deserve further research.

4. Experimental

4.1. Materials and instructions

All manipulations involving air-sensitive reagents were performed under an inert atmosphere of dry nitrogen. Tetrahydrofuran (THF) was dried over Na/benzophenone and distilled prior to use. All the intermediates were isolated,

analyzed by thin layer chromatography (TLC) on silica gel and ^{1}H NMR. All commercial materials, unless otherwise specified, were used as received.

^{1}H NMR spectra were recorded on a Bruker AV 300 spectrometer. Time-of-flight mass spectrometry (TOF-MS) was performed using a KOMPACT MALDI mass spectrometer (Shimadzu/Kratos) in the positive ion mode with dithranol as the matrix. The experimentally determined and calculated masses agree within the range of accuracy of the instrument. Elemental analysis was performed on a vario EL CHNS analyzer. UV–vis absorption spectra were obtained on an HP 8453 spectrophotometer. Photoluminescence spectra were measured using a Jobin–Yvon spectrofluorometer JY Fluorolog-3 spectrofluorometer.

Samples for TGA and DSC measurements were carefully dried to remove any residual solvent used in the work-up procedure. The absence of solvents was confirmed by ^{1}H NMR prior to analytical characterization. Thermal gravimetric analysis (TGA) was conducted on a TG 209 F1 (NETZSCH) thermal analysis system under a heating rate of 20 °C min^{-1}. Differential scanning calorimetry (DSC) was run on a DSC 204 F1 (NETZSCH) thermal analysis system. The sample was heated from −60 °C to 350 °C at a rate of 20 °C min^{-1}. Cyclic voltammetry was carried out on a CHI660A electrochemical workstation using platinum working electrode and Ag/AgCl reference electrode at a scan rate of 50 mV s^{-1} in nitrogen-saturated mixed solvents CH_2Cl_2/acetonitrile (5:1 v/v) containing 0.1 M *n*-Bu_4NPF_6. The Fc^+/Fc couple was used as internal standard. Ultraviolet photoemission spectroscopy (UPS) measurement was carried out using a Thermo Fish ESCA Lab 250 surface analysis system equipped with a He I (21.22 eV) gas discharge lamp. The base pressure of the analysis chamber was typically 2×10^{-8} Pa. The pass energy was 2.0 eV for obtaining the UPS spectra with an energy resolution of 0.10 eV. The vacuum level position of the spin-cast organic films was determined from the lowest inelastic electrons kinetic energy cutoff with a bias of −3.0 V for **1a**/**1c** and −6.0 V for **1b**. The position of Fermi edge was calibrated using a clean Ag film and all the spectra presented were plotted with respect to the determined Fermi level.

Compound **1c**. $Pd(PPh_3)_4$ (12 mg, 0.01 mmol) was added to a mixture of 4,7-dibromo-2,1,3-benzothiadiazole (0.1 g, 0.34 mmol) and 7-(3,6-di(1-naphthyl)carbazol-9-yl)-9,9-di-(*n*-octyl)fluoren-2-yl boronic ester (0.7 mg, 0.75 mmol) in toluene (30 mL), aqueous Na_2CO_3 (2 M, 4 mL) and ethanol (4 mL) under a nitrogen atmosphere [12c]. The reaction mixture was heated at 90 °C for 24 h. After being cooled to room temperature, it was diluted with distilled water. The organic layer was separated, dried over anhydrous $MgSO_4$, filtered and concentrated under reduced pressure. The residue was purified by column chromatography to afford a green solid. Yield: 0.37 g (62%). TLC R_f (3:1 petroleum ether/dichloromethane v/v): 0.31. ^{1}H NMR (300 MHz, $CDCl_3$, δ): 0.75–0.80 (m, 12H), 0.95–1.08 (m, 8H), 1.17–1.27 (m, 40H), 2.07–2.29 (m, 8H), 7.33–7.66 (m, 24H), 7.745–7.77 (m, 4H), 7.88–8.02 (m, 12H), 8.06–8.09 (m, 8H), 8.15 (d, 2H, J = 7.89 Hz), 8.32 (s, 4H). MALDI-TOF (*m*/*z*): $[M]^+$ calcd for $C_{128}H_{122}N_4S$, 1746.94; found, 1748.18 (100%). Anal. calcd for $C_{128}H_{122}N_4S$: C, 87.93; H, 7.05; N, 3.20; S, 1.83. found: C, 88.12; H, 6.75; N, 3.29; S, 1.86. T_d > 400 °C. $T_g \approx$ 105 °C (in the first heating run).

4.2. OLED fabrication and characterization

Two main types of OLEDs [ITO/PEDOT:PSS(50 nm)/PVK(***x*** nm)/**1a**–**1c**(45 nm)/ETL/LiF(1.5 nm)Al(200 nm) have been fabricated, where ***x*** = 0 nm (Type I) and 45 nm (Type II), ETL = Alq3 (30 nm) and TPBI (30 nm), respectively. For compound **1b**, double ETLs BCP (10 nm)/Alq3(20 nm) have been used to achieve hole confinement. The active emitters were spin-coated from a 20 mg mL^{-1} *p*-xylene solution at a speed of 2200 rpm. Patterned indium-tin oxide (ITO, 15 Ω/square)-coated glass substrates were cleaned successively with acetone, detergent, distilled water and 2-propanol in an ultrasonic bath. After treatment with oxygen plasma, PEDOT:PSS(4083) was spin-coated onto the ITO substrate and dried in a vacuum oven at 120 °C for 30 min. For the Type II OLEDs, PVK was coated on top of the PEDOT:PSS layer and dried at 100 °C for 15 min. Subsequently, thin films of the active emitters were spin-coated and dried at 100 °C for 10 min in the case of **1a** and **1c**, and 120 °C for **1b**. The organic electron-transport layers as well as the LiF electron-injection layer were deposited by vacuum thermal evaporation at a rate of 0.2 nm s^{-1} under a pressure of less than 5×10^{-4} Pa. The evaporation rate was monitored by a frequency counter and calibrated by Dektak 6 M Profiler (Veeco). The Al metallic cathode was evaporated at a higher rate of ~0.8–1 nm/s. Current density−brightness−voltage characteristics were measured by using Keithley source measurement units (Keithley 2400 and Keithley 2000) with a calibrated silicon photodiode. The EL spectra were measured by PR 650 spectrometer. The active area of device is 9 mm^2.

Acknowledgements

The authors Y.L., B.X.L. and W.Y.T. contribute equally to this work. X.H.Z. gratefully acknowledges the financial support of SCUT, NSF and MOST of China (Grant Nos. 2012ZZ0001, 51173051, 2009CB930604 & 2009CB623601) and wishes to thank Dr. Ya-Bing Qi at Princeton University and Dr. Miao Xuvery helpful discussion.

Appendix A. Supplementary data

Supplementary data associated with this article can be found, in the online version, at http://dx.doi.org/10.1016/j.orgel.2012.03.001.

References

[1] M. Shimizu, T. Hiyama, Chem. Asian J. 5 (2010) 1516.
[2] L. Duan, L.-D. Hou, T.-W. Lee, J. Qiao, D.-Q. Zhang, G.-F. Dong, L.-D. Wang, Y. Qiu, J. Mater. Chem. 20 (2010) 6392.
[3] X.-H. Zhu, J.B. Peng, Y. Cao, J. Roncali, Chem. Soc. Rev. 40 (2011) 3509.
[4] T.S. Qin, W. Wiedemair, S. Nau, R. Trattnig, S. Sax, S. Winkler, A. Vollmer, N. Koch, M. Baumgarten, E.J.W. List, K. Muellen, J. Am. Chem. Soc. 133 (2011) 1301.
[5] [a] P. Sonar, M.-S. Soh, Y.-H. Cheng, J.-T. Henssler, A. Sellinger, Org. Lett. 12 (2010) 3293;
[b] M.-Y. Lo, C.-G. Zhen, M. Lauters, G.E. Jabbour, A. Sellinger, J. Am. Chem. Soc. 129 (2007) 5808.

[6] [a] Y.J. Pu, M. Higashidate, K.I. Nakayama, J. Kido, J. Mater. Chem. 18 (2008) 4183;
[b] J.-H. Huang, J.-H. Su, X. Li, M.-K. Lam, K.-M. Fung, H.-H. Fan, K.-W. Cheah, C.-H. Chen, H. Tian, J. Mater. Chem. 21 (2011) 2957;
[c] I. Cho, S.H. Kim, J.H. Kim, S. Park, S.Y. Park, J. Mater. Chem. 22 (2012) 123.
[7] M. Zhang, S. Xue, W. Dong, Q. Wang, T. Fei, C. Gu, Y.-G. Ma, Chem. Commun. 46 (2010) 3923.
[8] G. Barbarella, L. Favaretto, A. Zanelli, G. Gigli, M. Mazzeo, M. Anni, A. Bongini, Adv. Funct. Mater. 15 (2005) 664.
[9] [a] C.-G. Zhen, Y.-F. Dai, W.-J. Zeng, Z. Ma, Z.-K. Chen, J. Kieffer, Adv. Funct. Mater. 21 (2011) 699;
[b] L. Wang, Y. Jiang, J. Luo, Y. Zhou, J. Zhou, J. Wang, J. Pei, Y. Cao, Adv. Mater. 21 (2009) 4854.
[10] F. Liu, C. Tang, Q.-Q. Chen, S.-Z. Li, H.-B. Wu, L.-H. Xie, B. Peng, W. Wei, Y. Cao, W. Huang, Org. Electron. 10 (2009) 256.
[11] Z.-C. Ding, R.-B. Xing, Q.-A. Fu, D.-G. Ma, Y.-C. Han, Org. Electron. 12 (2011) 703.
[12] [a] J. Huang, Q. Liu, J.-H. Zou, X.-H. Zhu, A.-Y. Li, J.-W. Li, S. Wu, J.B. Peng, Y. Cao, R. Xia, D.D.C. Bradley, J. Roncali, Adv. Funct. Mater. 19 (2009) 2978;
[b] L. Zhao, J.-H. Zou, J. Huang, C. Li, Y. Zhang, C. Sun, X.-H. Zhu, J.B. Peng, Y. Cao, J. Roncali, Org. Electron. 9 (2008) 649;
[c] Y. Li, A.-Y. Li, B.-X. Li, J. Huang, L. Zhao, B.-Z. Wang, J.-W. Li, X.-H. Zhu, J.B. Peng, Y. Cao, D.-G. Ma, J. Roncali, Org. Lett. 11 (2009) 5318.
[13] [a] C.W. Tang, S.A. VanSlyke, Appl. Phys. Lett. 51 (1987) 913;
[b] Y. Shirota, H. Kageyama, Chem. Rev. 107 (2007) 953.
[14] [a] Z.-J. Zhao, S.-M. Chen, J.W.Y. Lam, Z.-M. Wang, P. Lu, F. Mahtab, H.H.Y. Sung, I.D. Williams, Y.-G. Ma, H.-S. Kwok, B.-Z. Tang, J. Mater. Chem. 21 (2011) 7210;
[b] Z.-Y. Xia, J.-H. Su, H.-H. Fan, K.-W. Cheah, H. Tian, C.-H. Chen, J. Phys. Chem. C 114 (2010) 11602;
[c] A.P. Kulkami, Y. Zhu, A. Babel, P.-T. Wu, S.A. Jenekhe, Chem. Mater. 20 (2008) 4212;
[d] Q.-X. Tong, S.-L. Lai, M.-Y. Chan, K.-H. Lai, J.-X. Tang, C.-S. Lee, S.-T. Lee, Appl. Phys. Lett. 91 (2007) 153504.
[15] A.J. Mäkinen, I.G. Hill, Z.H. Kafafic, J. Appl. Phys. 92 (2002) 1598.
[16] Y.-Q. Li, M.-K. Fung, Z.-Y. Xie, S.-T. Lee, L.-S. Hung, J.-M. Shi, Adv. Mater. 14 (2002) 1317.
[17] [a] L. Zhou, H.-J. Zhang, R.-P. Deng, Z.-Y. Guo, J. Feng, Z.-F. Li, J. Phys. Chem. C 112 (2008) 15065;
[b] H.-Q. Tang, H.-X. Liao, L.-H. Zhu, Chem. Phys. Lett. 381 (2003) 605.
[18] [a] A.J. Campbell, D.D.C. Bradley, H. Antoniadis, J. Appl. Phys. 89 (2001) 3343;
[b] T. van Woudenbergh, J. Wildeman, P.W.M. Blom, J.J.A.M. Bastiaansen, B.M.W. Langeveld-Voss, Adv. Funct. Mater. 14 (2004) 677.
[19] X.-F. Qiao, Y.-T. Tao, Q. Wang, D.-G. Ma, C.-L. Yang, L.-X. Wang, J.-G. Qin, F.-S. Wang, J. Appl. Phys. 108 (2010) 034508.
[20] F. Cacialli, R.H. Friend, N. Haylett, R. Daik, W.J. Feast, D.A. dos Santos, J.L. Brédas, Appl. Phys. Lett. 69 (1996) 3794.
[21] [a] M.B. Khalifa, D. Vaufrey, A. Bouazizi, J. Tardy, H. Maaref, Mater. Sci. Eng. C 21 (2002) 277;
[b] Y.-G. Zhang, Y.-F. Hu, J.-S. Chen, Q.-G. Zhou, D.-G. Ma, J. Phys. D: Appl. Phys. 36 (2003) 2006.